

pH-Sensitive Niosomal Nanoencapsulation of Beta-Caryophyllene and its Novel Pathway in Triple Negative Breast Cancer

Ebrahim Sadaqa ¹, Arif Setiawansyah ^{2,*}, Muhammad Ikhlas Arsul ³, Bambang Hernawan Nugroho ⁴, Sjaikhurrizal El Muttaqien ⁵, Fitria Dwi Ayuningtyas ⁶, Nurul Hidayati ²

¹ Doctoral Student at Department of Pharmaceutics, School of Pharmacy, Bandung Institute of Technology, Bandung, Indonesia; 30722701@mahasiswa.itb.ac.id

² Center of Natural Product Extract Laboratory, Cendikia Farma Husada Pharmacy Academy, Indonesia; setiawansyah@akfarcefada.ac.id (A.S.); nurulhidayati.cefada@gmail.com (N.H.);

³ Department of Pharmacy, Faculty of Health Sciences, Universitas Islam Negeri Alauddin, Gowa, Indonesia; ikhlas.arsul@uin-alauddin.ac.id

⁴ Department of Pharmacy, Faculty of Mathematics and Science, Universitas Islam Indonesia, Indonesia; bambang.hernawan@uii.ac.id

⁵ Research Center for Vaccine and Drugs, National Research and Innovation Agency (BRIN), LAPTIAB 1, PUSPIPTEK, Tangerang Selatan 15314, Indonesia; sjai001@brin.go.id

⁶ Scientific Imaging Center, Bandung Institute of Technology, Indonesia; fitria.ayuningtyas@itb.ac.id;

* Correspondence: setiawansyah@akfarcefada.ac.id (AS)

Scopus Author ID 58628290500

Received: 31.12.2024; Accepted: 11.04.2025; Published: 8.06.2025

Abstract: Triple-negative breast cancer (TNBC) is an aggressive malignancy requiring innovative therapies. This study aimed to develop a pH-sensitive hybrid niosomal beta-caryophyllene (BCP) formulation to overcome its delivery limitations and leverage a novel anticancer pathway using *in silico* tools. Using *in silico* methods, HSP90AA1 was identified as a key TNBC target, with network pharmacology, molecular docking, and dynamics confirming the stable binding of BCP. Hybrid niosomes were prepared via a thin-film hydration method with PLGA modification to enhance pH-sensitive delivery. The formulations were characterized for particle size, encapsulation efficiency, and drug release profiles, while cytotoxicity was evaluated using the CCK-8 assay in 4T1 TNBC cells. PLGA-modified niosomes achieved a particle size of 187.6 ± 7.82 nm, $91.96 \pm 2.71\%$ encapsulation efficiency, and exhibited pH-responsive release, significantly increasing BCP release at pH 5.5 compared to pH 7.4. The hybrid formulation demonstrated superior cytotoxicity (IC_{50} : 15.65 ± 6.19 μ g/mL), representing a 4.61-fold improvement compared to free BCP and a 1.96-fold enhancement over standard niosomes. Leveraging the novel BCP-HSP90AA1 pathway enhanced anticancer efficacy, showcasing a promising strategy for TNBC treatment. This study integrates computational and experimental approaches to address BCP's delivery challenges, highlighting the potential of PLGA-modified niosomes as a targeted TNBC therapy.

Keywords: beta-caryophyllene; HSP90AA1; molecular docking; molecular dynamics simulation; niosomes; pH-sensitive drug delivery; targeted cancer therapy.

© 2025 by the authors. This article is an open-access article distributed under the terms and conditions of the Creative Commons Attribution (CC BY) license (<https://creativecommons.org/licenses/by/4.0/>), which permits unrestricted use, distribution, and reproduction in any medium, provided the original work is properly cited. The authors retain the copyright of their work, and no permission is required from the authors or the publisher to reuse or distribute this article as long as proper attribution is given to the original source.

1. Introduction

Beta-caryophyllene (BCP), a naturally occurring sesquiterpene found in essential oils such as clove, oregano, and cannabis, has garnered attention as a versatile bioactive compound with notable anti-inflammatory, analgesic, and anticancer properties [1]. BCP exerts its anticancer effects by inducing apoptosis, inhibiting cancer cell proliferation, and modulating pivotal signaling pathways such as NF- κ B and PI3K/Akt/mTOR, which play critical roles in tumor progression [2–4]. However, these signaling pathways are often associated with therapy resistance and pathway redundancy, limiting the effectiveness of conventional treatments targeting these mechanisms [5–7]. This highlights a critical gap in understanding BCP's full anticancer potential, particularly its ability to modulate alternative pathways and molecular targets.

Despite its promising biological activity, the clinical translation of BCP is hindered by significant formulation challenges, including poor aqueous solubility, rapid systemic clearance, and low bioavailability. These physicochemical limitations severely restrict its therapeutic efficacy, particularly in systemic applications such as cancer therapy [8]. Current research has predominantly focused on improving the bioavailability of hydrophobic compounds like BCP through encapsulation strategies. Yet, innovative solutions capable of overcoming these barriers while enabling precise, targeted delivery remain underexplored. Niosomes, self-assembling, non-ionic surfactant-based vesicles, have shown potential in addressing such challenges. Their ability to enhance drug solubility, prolong circulation time, and facilitate targeted delivery makes them a promising platform for hydrophobic drug encapsulation [9]. However, standard niosomal formulations often lack the stimuli-responsive properties needed for effective drug release in the unique tumor microenvironment, such as the acidic pH resulting from the Warburg effect.

This study bridges this critical gap by introducing a hybrid polymeric niosomal formulation. The niosomes are modified with the biodegradable polymer poly(lactic-co-glycolic acid) (PLGA) to impart pH-sensitive properties, enabling precise and enhanced drug release in the acidic microenvironment of triple-negative breast cancer (TNBC) tumors. TNBC, characterized by its aggressive nature and lack of targeted therapies, presents a compelling model to evaluate the potential of such advanced drug delivery systems [10,11]. In addition to addressing the formulation challenges of BCP, this study employs a comprehensive integrative approach to explore its anticancer mechanisms. Using network pharmacology, molecular docking, and molecular dynamics (MD) simulations, we systematically identify novel molecular targets and pathways modulated by BCP [12].

The distinctive contributions of this study center on developing a pH-sensitive, polymer-enhanced niosomal system that addresses critical barriers in drug delivery for BCP. This formulation not only improves the solubility and bioavailability of BCP but also leverages the acidic microenvironment of tumors for precise, controlled drug release. By seamlessly integrating advanced computational techniques such as network pharmacology, molecular docking, and molecular dynamics simulations with experimental validation, this research provides a comprehensive framework for exploring the therapeutic potential of naturally derived compounds like BCP. A key focus of this study is the identification of novel anticancer pathways and molecular targets modulated by BCP. Through computational modeling, we uncover alternative mechanisms of action beyond conventional signaling pathways, offering insights into how BCP can circumvent therapy resistance in TNBC. These findings enhance

our understanding of BCP's multifaceted role in cancer treatment and underscore the potential for systems-level analyses to guide the rational design of targeted therapies. By bridging computational insights with experimental validation, this work lays the groundwork for future advancements in hybrid drug delivery systems. It highlights the transformative role of systems-based computational approaches in precision oncology, facilitating the clinical translation of bioactive compounds into effective therapeutic strategies for aggressive cancers like TNBC. The findings presented here exemplify how interdisciplinary approaches can address unmet therapeutic needs and pave the way for more effective and personalized cancer treatments.

2. Materials and Methods

2.1. Materials.

Beta-caryophyllene, cholesterol, Span 60 (sorbitan monostearate), poly(lactic-co-glycolic acid) (PLGA; 50:50 composition, inherent viscosity: 0.4 dL/g), chloroform, methanol, and the Cell Counting Kit-8 (CCK-8) were obtained from Sigma-Aldrich (St. Louis, MO, USA). Dulbecco's Modified Eagle Medium (DMEM, high glucose), fetal bovine serum (FBS, premium grade), penicillin-streptomycin, trypsin-EDTA solution, and phosphate-buffered saline (PBS, pH 7.4) were purchased from Gibco, Thermo Fisher Scientific (Waltham, MA, USA). The 4T1 mouse mammary carcinoma cells (ATCC® CRL-2539) were kindly provided by Dr. Nurul Utami from the Department of Histology, Faculty of Medicine, Universitas Lampung, Indonesia. Molecular dynamics simulations were conducted on a dedicated workstation running Ubuntu 20.04 LTS. The system featured an Intel® Core™ i9-12900KF processor (24 CPU at 3.6 GHz), 32 GB of RAM, and an NVIDIA RTX 4060 GPU with 16 GB VRAM. GROMACS 2022.3 was utilized as the molecular dynamics software.

2.2. Network pharmacology study.

The computational target prediction workflow began with the analysis of compounds' canonical SMILES structures using the SuperPRED database (<https://prediction.charite.de>). The predicted gene targets were validated and standardized through the UniProt database (<https://www.uniprot.org>), then cross-referenced with triple-negative breast cancer-associated genes from GeneCards (<https://www.genecards.org>) using the Venny 2.0 intersection tool (<https://bioinfogp.cnb.csic.es/tools/venny/>). Subsequently, protein-protein interaction (PPI) networks were constructed using the STRING database (<https://string-db.org>), followed by network visualization and topological parameter analysis in Cytoscape 3.10.1. The identified core targets were then subjected to pathway enrichment and biological process analyses using ShinyGO 0.80 (<http://bioinformatics.sdstate.edu/go/>). All enrichment analyses were conducted with a false discovery rate (FDR) cut-off 0.05.

2.3. Molecular docking study.

The molecular docking investigation was conducted utilizing Autodock 4.2 via the ADT interface (The Scripps Research Institute), with HSP90AA1 as the target macromolecule based on network pharmacology findings. The protocol initiated the structural preparation of both components: HSP90AA1 co-crystal structure (obtained from PDB, ID: 5H22) and BCP 3D structure (sourced from PubChem, CID: 5281515). Protein preparation was executed in Biovia Discovery Studio Visualizer 2021, involving the removal of water molecules, native

ligands, heteroatoms, and non-essential chains. The BCP structure underwent energy minimization using MM2 energy minimization in Chem3D Pro, with subsequent configuration of rotatable bonds and center nodes in ADT. Grid box parameters were optimized to encompass HSP90AA1's active site region adequately. The docking simulation implemented a flexible-rigid methodology, utilizing genetic algorithm parameters to generate 100 conformations with Lamarckian GA output. The entire docking protocol was executed in ten repetitions to ensure reliability.

2.4. Molecular dynamic simulation.

Molecular dynamics (MD) simulations were performed using the GROMACS software package. The system was parameterized using the CHARMM36m force field for the protein component and the CHARMM General Force Field (CGenFF) for the ligand. Solvation was carried out in an octahedral TIP3P water box, and Na⁺ and Cl⁻ ions were added to neutralize the system and mimic physiological ionic conditions. The simulation workflow included systematic energy minimization to resolve steric clashes, followed by equilibration under constant volume (NVT) and constant pressure (NPT) ensembles. The temperature was maintained at 310 K using the velocity rescaling thermostat, and the pressure was controlled at 1 atm using the Parrinello-Rahman barostat. Long-range electrostatic interactions were computed using the Particle Mesh Ewald algorithm. The production MD simulation was run for 200 ns, and trajectory analyses were performed to evaluate root mean square deviation (RMSD), root mean square fluctuation (RMSF), solvent-accessible surface area (SASA), radius of gyration (Rg), and hydrogen bond dynamics. All analyses were conducted using GROMACS tools. Structural visualization and trajectory inspection were carried out using Chimera and Biovia Discovery Studio.

2.5. Preparation of BCP encapsulated niosome.

BCP-encapsulated niosomes were prepared using a modified thin-film hydration method based on the protocol by Zolghadri *et al.* [13]. Cholesterol and Span 60 were combined in a 1:1 molar ratio to achieve a final Span 60 concentration of 10 mM, which exceeds its critical micelle concentration (CMC), ensuring optimal vesicle formation [14]. BCP at a concentration of 200 µg/mL was co-dissolved with the lipid components in a chloroform:methanol mixture (2:1 v/v) in a round-bottom flask. The solvent mixture was evaporated under reduced pressure at 40°C using a rotary evaporator, creating a uniform thin lipid film on the inner surface of the flask. This film was then hydrated with phosphate-buffered saline (PBS, pH 7.4) to produce a niosomal dispersion. Hydration was carried out at room temperature with gentle swirling for 30 minutes to facilitate the complete formation of vesicles. The resulting niosomal suspension was sonicated using a probe sonicator for 10 minutes to ensure uniform vesicle size and to enhance the encapsulation efficiency of BCP. To develop hybrid polymeric niosomes, PLGA (0.1% w/v) was incorporated into the organic phase before thin-film formation to introduce pH-sensitive properties. Both standard niosomal and hybrid polymeric niosomal formulations containing BCP at a concentration of 200 µg/mL were stored at 4°C to maintain stability. All formulations were prepared in triplicate to ensure reproducibility. The particle size, polydispersity index (PDI), and zeta potential of the prepared niosomes were determined using dynamic light scattering (DLS) and zeta potential analysis. These measurements were conducted with a particle size analyzer (Beckman Coulter, West

Sacramento, CA, USA) and a zeta potential analyzer (Malvern Instruments, Malvern, UK), ensuring precise and reproducible results.

2.6. Determination of entrapment efficiency (EE).

The entrapment efficiency of BCP-encapsulated niosomes was calculated using the ultrafiltration centrifugation method described by previous research [15] with modifications. In brief, niosomal suspensions were transferred into Amicon Ultra-15 centrifugal filter units equipped with Ultracel regenerated cellulose membranes having a molecular weight cut-off (MWCO) of 30,000 Da. These units effectively retain niosomal vesicles while allowing free BCP to pass through the membrane. The samples were centrifuged at $10,000 \times g$ for 60 minutes at 4°C to separate free BCP from the encapsulated form. The filtrate, containing unencapsulated BCP, was collected and analyzed using a T92+ UV-visible spectrophotometer (PG Instruments, Lutterworth, UK) at 205 nm, referencing a pre-established calibration curve for BCP.

The entrapment efficiency was calculated using the formula:

$$EE (\%) = \left(\frac{\text{Total BCP added} - \text{Free BCP in filtrate}}{\text{Total BCP added}} \right) \times 100 \quad (1)$$

All measurements were performed in triplicate, and results were reported as mean values with standard deviations to ensure accuracy and reproducibility.

2.7. In vitro release test.

The in vitro release profile of BCP from standard niosomes (BCP-NIO) and hybrid polymeric niosomes (BCP-PLGA-NIO) was assessed under conditions simulating the physiological environment (pH 7.4) and the acidic tumor microenvironment (pH 5.5). For each release study, 5 mL of the niosomal suspension, containing a total of 1,000 μg of BCP (with a concentration of 200 $\mu\text{g}/\text{mL}$), was loaded into dialysis bags (molecular weight cut-off, MWCO 12–14 kDa). These dialysis bags were securely sealed and then immersed in 50 mL of phosphate-buffered saline (PBS) at the respective pH values. The setup was maintained at 37°C with constant stirring at 100 rpm to replicate physiological conditions. At predetermined intervals (1, 2, 3, 4, 5, 6, 7, 8, 12, and 24 hours), 1 mL of the external release medium were withdrawn for analysis and immediately replaced with an equivalent fresh PBS to maintain sink conditions. The concentration of BCP in the collected samples was quantified using a T92+ UV-visible spectrophotometer (PG Instruments, Lutterworth, UK), with measurements taken at 205 nm. Calibration curves prepared for BCP in PBS (pH 5.5 and 7.4) were used to accurately calculate the released drug concentrations. All release experiments were conducted in triplicate, and cumulative release data were analyzed to evaluate the release behavior of BCP from the different niosomal formulations under varying pH conditions.

2.8. Cell culture.

4T1 breast cancer cells were cultured in DMEM supplemented with 10% FBS and 1% penicillin-streptomycin at 37°C in a 5% CO_2 incubator. At 80–90% confluency, cells were washed with PBS and detached using trypsin-EDTA for subsequent experiments.

2.9. *In vitro* cytotoxicity assay.

The cytotoxic effects of free BCP, BCP-NIO, and BCP-PLGA-NIO were assessed using the CCK-8 assay as previously described by Sadaqa *et al.* [16]. In brief, 4T1 cells were seeded at a density of 5×10^3 cells/well in 96-well plates containing 100 μ L of DMEM supplemented with 10% FBS and 1% penicillin-streptomycin and incubated at 37°C with 5% CO₂ for 24 hours. Following incubation, cells were treated with six concentrations of each formulation (ranging from 150 μ g/mL to 1.171 μ g/mL, prepared through serial dilutions) and incubated for 24 hours. Untreated cells served as the negative control. After treatment, 10 μ L of CCK-8 solution was added to each well, and the plates were incubated at 37°C for 1 hour. The absorbance was measured at 450 nm using a microplate reader to determine cell viability. All experiments were performed in triplicate, and results were expressed as mean \pm SD. The inhibitory concentration (IC₅₀) values for each formulation were calculated using CompuSyn software, enabling a comparative cytotoxicity analysis across the tested formulations.

3. Results and Discussion

3.1. Network pharmacology study.

The molecular mechanism of BCP in combating TNBC was evaluated using a network pharmacology approach by observing BCP’s target genes, which are associated with TNBC and its Kyoto Encyclopedia of Genes and Genomes (KEGG) pathways, as well as the gene ontology biological process. Figure 1 displays the gene mining results from BCP associated with TNBC, *their interactions*, and the core target genes. During the observation, 151 genes from BCP and 1081 TNBC-related genes were found, undergoing cross-match, resulting in 74 common genes, as depicted in Figure 1a. These genes illustrated interconnection to each other with a different number of connectivities (Figure 1b); the highest degree of connectivity shown in purple, which is represented by 32 nodes of connections, was observed at HSP90AA1, ESR1, and PPARG. Topological analysis exhibited ten core targets, as Figure 1c, including HSP90AA1, ESR1, PPARG, PTGS2, NFKB1, AR, TLR4, PGR, NR3C1, and TERT. Their high degree of connectivity indicates that these genes might have an essential role in TNBC.

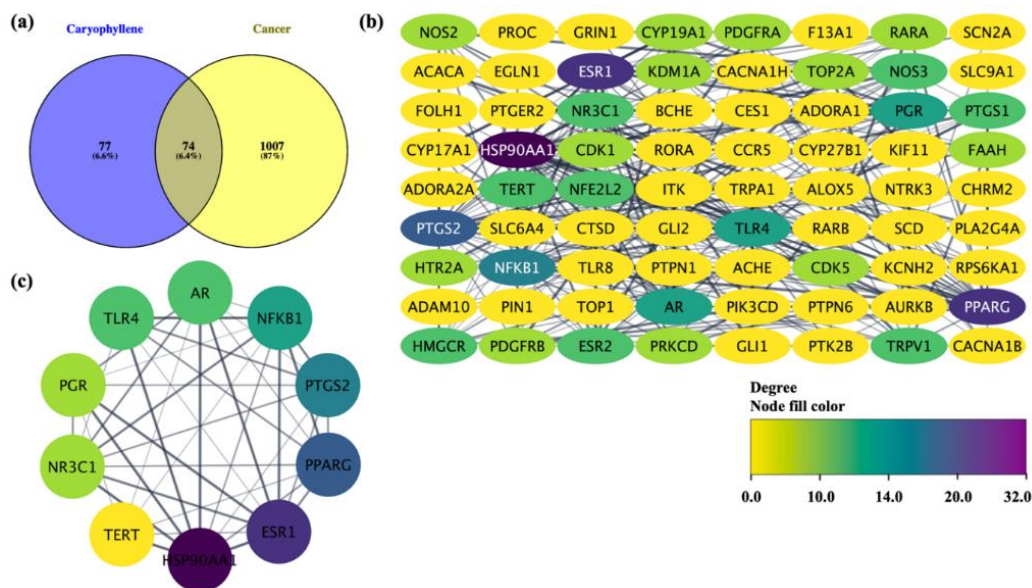


Figure 1. Target identification results of BCP and TNBC-related genes. (a) Venn diagram of cross-match of BCP and TNBC-related genes; (b) PPIs network of common genes from BCP and TNBC; (c) the core target genes.

The core targets were further used for KEGG enrichment and gene ontology biological process. The result, depicted in Figure 2, demonstrates the potential pathway of BCP in TNBC by regulating mammary gland duct morphogenesis and cell death through HSP90AA1. In KEGG pathway analysis, IL-17 and NF- κ B signaling pathways were highly enriched, while the estrogen signaling pathway was moderate (Figure 2a). These pathways are well-known to be associated with TNBC, which can trigger its initiation, growth, and metastasis. Furthermore, the network construction of BCP-disease genes, presented in Figure 2c, illustrates the involvement of HSP90AA1 as one of the contributors to breast cancer, highlighting its potential in TNBC tumorigenesis. As a consequence, HSP90AA1 was considered as the main target of this work.

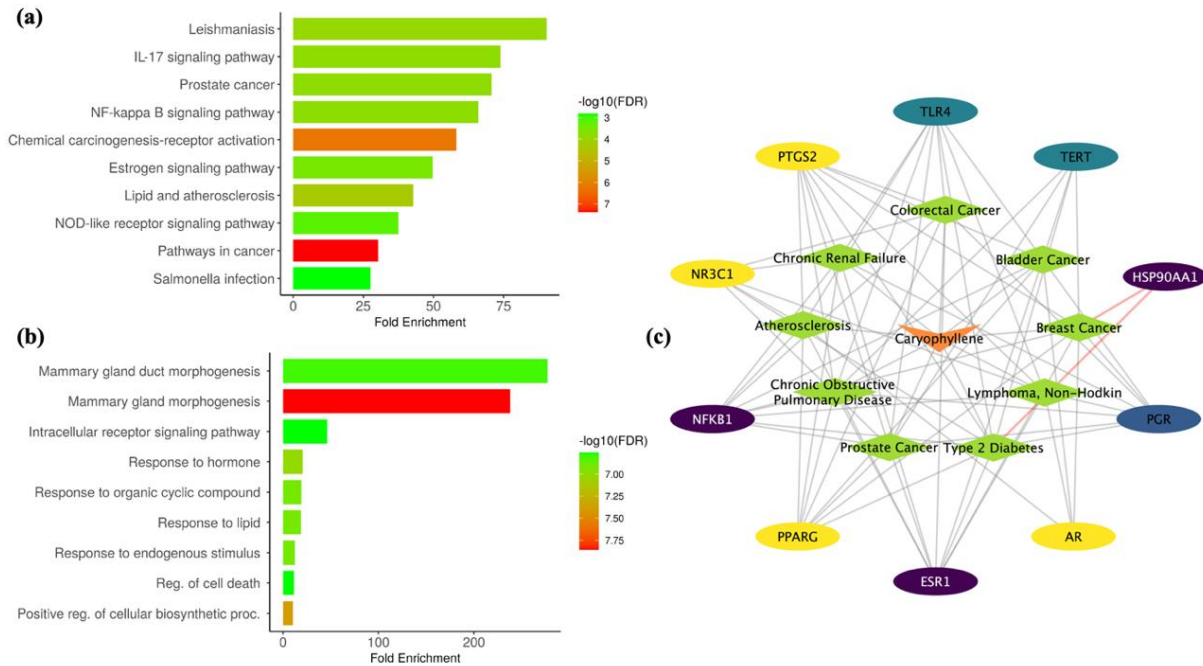


Figure 2. The network analysis of the core targets. **(a)** KEGG enrichment; **(b)** Gene ontology biological process; **(c)** BCP-diseases-gene network.

HSP90AA1 emerges as a critical molecular protagonist significantly influencing TNBC's intricate pathogenesis and progression. HSP90AA1 demonstrates remarkable oncogenic capabilities by stabilizing and protecting key signaling proteins involved in cell proliferation, survival, and metastasis. HSP90AA1 is a critical guardian of multiple oncogenic client proteins, including mutant p53, AKT, RAF kinases, and multiple receptor tyrosine kinases [17–19]. When destabilized, these proteins typically undergo proteasomal degradation; however, HSP90AA1's chaperoning function prevents this process, thereby promoting cancer cell survival and resistance to therapeutic interventions. The metastatic potential of TNBC is particularly enhanced by HSP90AA1's intricate involvement in cellular migration and invasion mechanisms. Studies by Tian *et al.* [20] demonstrated that HSP90AA1 modulates epithelial-mesenchymal transition (EMT) through stabilizing key transcription factors and signaling molecules. This molecular manipulation facilitates cancer cell detachment, enhanced motility, and metastatic dissemination.

Furthermore, HSP90AA1 contributes to the maintenance of cancer stem cell populations, which are inherently responsible for tumor initiation, therapeutic resistance, and metastatic colonization. Emerging therapeutic strategies targeting HSP90AA1 represent a promising approach to combating TNBC's aggressive nature. A groundbreaking investigation by Eisa *et al.* [21] revealed that HSP90AA1 inhibition induces profound proteotoxic stress,

On the realm of potential inhibition of BCP to HSP90AA1, Figure 3b displays the binding energy of BCP compared to the native ligand and Sorafenib. Even though BCP demonstrated less negative binding energy (-5.80 ± 0.206 kcal/mol) than the native ligand (-9.63 ± 0.194 kcal/mol), its binding energy was significantly more negative than Sorafenib (-4.97 ± 0.833 kcal/mol), indicating BCP had better affinity to HSP90AA1 compared to Sorafenib. The stronger binding affinity of BCP can be attributed to its compact structure and specific interaction pattern. BCP formed key hydrophobic interactions with residues, including Leu 107, Val 186, and Phe 138, creating a stable binding pose within the pocket. Additionally, the presence of Met 98 and Ala 55 in proximity to BCP suggested potential pi-alkyl interactions that further stabilize the complex. This finding aligns with previous research by Wright *et al.* [23] and Dernovsek *et al.* [24], who demonstrated that smaller molecules with optimal hydrophobic interactions often achieve better binding stability with HSP90AA. This is also corroborated by the findings of Susianti *et al.* [25], which highlighted that smaller molecules like mono and sesquiterpenoids tended to be well-bounded with the active site of the proteins.

In contrast, Sorafenib displayed a more extensive interaction network but potentially less optimal binding. While it formed multiple interactions with residues such as hydrogen bonds (Asn 51, Gly 97, Lys 58), pi-alkyl (Val 186, Phe 138, Ala 55, Met 98, Ile 96, Ile 110), pi-sulfur (Met 98), and pi-anion (Asp 102), its larger structure and more complex interaction pattern may contribute to reduced binding specificity. This observation corresponds with findings from Smith *et al.* (2012) [26], who reported that larger molecules might experience reduced binding efficiency despite forming numerous interactions due to increased entropy penalties and potential steric hindrance. The superior binding affinity of caryophyllene can be further explained by the "lock-and-key" principle in molecular recognition. The compact structure of caryophyllene appears to achieve an optimal fit within the binding pocket, maximizing interaction efficiency while minimizing entropy loss. Smaller molecules like BCP often achieve better binding scores due to their ability to maintain specific, high-quality interactions without the entropic penalties associated with larger, more flexible ligands [27].

MD simulation over 200 ns confirmed this high potential, which shows BCP-HSP90AA1 complex stability and flexibility. Figure 4 showcases the dynamic nature of complex BCP-HSP90AA1 compared to Sorafenib and the native ligand. In general, BCP exhibited excellent binding stability for both the entire structure and individual residues to HSP90AA1 compared to Sorafenib over 200 ns simulation. The RMSD value of BCP, presented in Figure 4a, illustrated a fluctuation in the first 50 ns and is more likely to be stable for the rest of the simulation time. A similar phenomenon was also observed in Sorafenib, which showed a tendency to fluctuate from 0 – 50 ns, followed by a 150 ns period of stability. However, the RMSD value of BCP was slightly better than Sorafenib's, suggesting that BCP demonstrated fewer conformational changes and had excellent system stability during simulation [28]. Less conformational changes of BCP were more likely to occur due to its rigidity, which was indicated by the lack of a rotatable bond within the structure. Moreover, this stability was observed entirely from the system and the individual residues, as depicted in Figure 4b. The RMSF value of BCP was better than both native ligands and Sorafenib in the overall 200 ns simulation, suggesting BCP tended to interact with the same particular residues of the HSP90AA1 binding pocket.

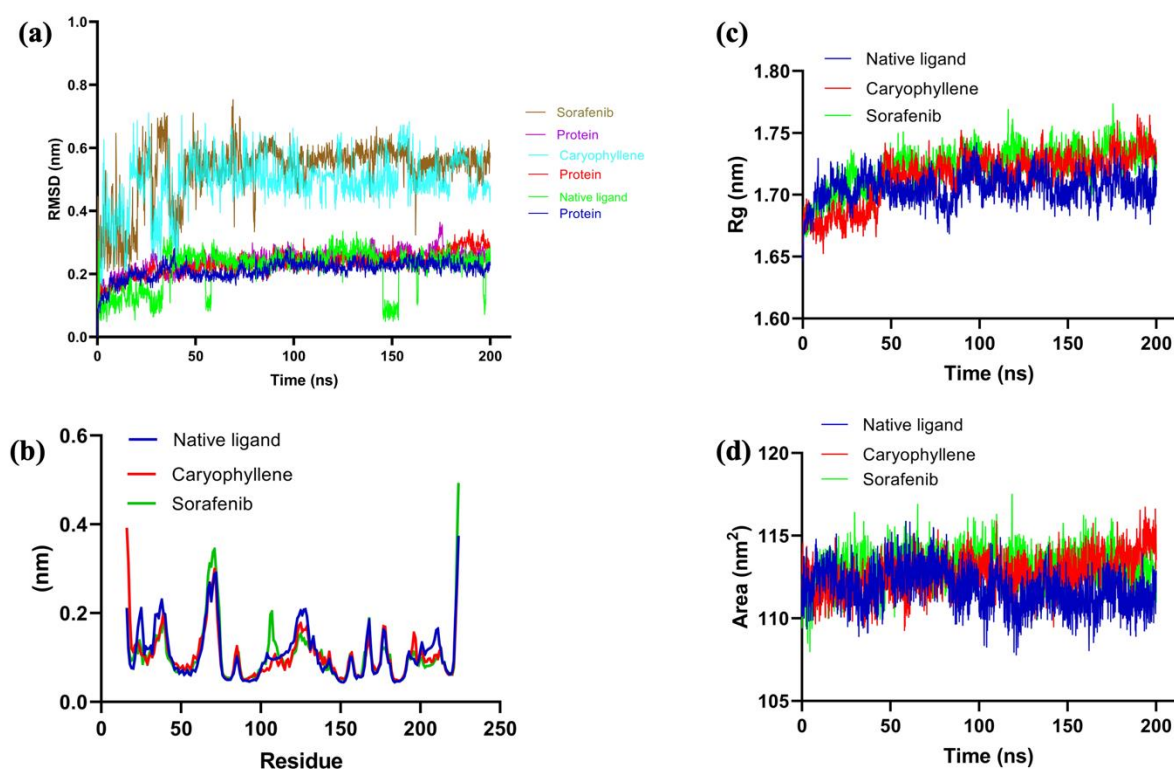


Figure 4. Molecular dynamic simulation results over 200 ns. (a) RMSD; (b) RMSF; (c) Radius of gyration; (d) SASA.

The effect of BCP on HSP90AA1 structure compactness was also measured by observing the radius of gyration (Rg) value during the simulation; the higher the Rg, the more compact the protein structure is going to be [29]. Figure 4c displays the Rg value of BCP, Sorafenib, and native ligands over 200 ns of MD simulation. Overall, BCP had an increased Rg in a particular period, which was followed by a flat Rg for the rest of the simulation, while Sorafenib and native ligand demonstrated an unchanged Rg value. In detail, BCP had the lowest Rg value in the first 50 ns compared to the native ligand and Sorafenib, which grew more after with the Rg value greater than the native ligand yet lower than Sorafenib. This demonstrated that BCP dropped the HSP90AA1's compactness, destabilizing HSP90AA1's integrity better than Sorafenib. On the realm of solvent-accessible surface area (SASA), presented in Figure 4d, BCP had an overall SASA value lower than Sorafenib, yet higher than native ligand, indicating Sorafenib possessed more surface area exposed to solvent than BCP, making Sorafenib-HSP90AA1 complex more flexible and more amenable to drug binding. However, the extensive surface area results in non-specific binding between the ligand and the protein's active site, thereby reducing its capacity to exert biological effects [30–32]. This diminished specificity in molecular interactions potentially compromises the compound's therapeutic efficacy. Numerous studies indicated a potential correlation between SASA values and drug resistance mechanisms. Higher SASA protein values may contribute to increased drug resistance, as the expanded surface area available for drug interactions can paradoxically impede effective drug binding. The greater binding surface area may reduce the likelihood of stable and specific drug-protein interactions, potentially diminishing therapeutic efficacy [33,34]. Accordingly, BCP had much better binding stability and specificity to HSP90AA1 than Sorafenib, strengthening the overall finding from the molecular docking and dynamic simulation.

3.3. Formulation pH-sensitive niosomal encapsulation of BCP.

3.3.1. Physicochemical characterization.

The physicochemical properties of the niosomal formulations were thoroughly evaluated to assess their suitability for encapsulating BCP and enhancing its therapeutic potential. As summarized in Table 1, the mean particle size of BCP-NIO was 130.8 ± 9.80 nm, whereas the incorporation of PLGA increased the particle size to 187.6 ± 7.82 nm. This increase in size can be attributed to the addition of the polymer layer, which enhances structural complexity and vesicle stability. Despite the larger size of BCP-PLGA-NIO, both formulations exhibited a low polydispersity index (PDI), with values of 0.210 ± 0.048 for BCP-NIO and 0.265 ± 0.002 for BCP-PLGA-NIO, indicating uniform size distribution.

Table 1. Physicochemical characteristics of BCP-encapsulated niosomes and PLGA-modified niosomes.

Groups	Mean droplet particle size (nm)	Mean polydispersity index (PDI)	Mean Zeta Potential (mV)
BCP-NIO	130.8 ± 9.80	0.210 ± 0.048	-12.67 ± 2.70
BCP-PLGA-NIO	187.6 ± 7.82	0.265 ± 0.002	-20.05 ± 8.90

The zeta potential values, also presented in Table 1, revealed a notable difference between the two formulations. BCP-NIO exhibited a zeta potential of -12.67 ± 2.70 mV, while the PLGA-modified niosomes displayed a higher negative charge of -20.05 ± 8.90 mV. The increased negative surface charge in BCP-PLGA-NIO likely arises from the anionic nature of PLGA, which enhances electrostatic repulsion among vesicles, thereby improving colloidal stability [35]. This property is particularly advantageous for maintaining vesicle integrity during systemic circulation, reducing aggregation, and increasing the likelihood of efficient tumor targeting. Improved colloidal stability is a key parameter in ensuring that the niosomes remain intact until they reach the targeted site, such as the acidic microenvironment of triple-negative breast cancer (TNBC) tumors. EE analysis demonstrated that both formulations were highly effective in encapsulating BCP, with BCP-PLGA-NIO achieving a significantly higher EE of 91.96 ± 2.71 % compared to 88.23 ± 5.63 % for BCP-NIO (Table 1). The enhanced EE of BCP-PLGA-NIO highlights the role of PLGA in stabilizing the hydrophobic core of the niosomal structure, thereby reducing drug leakage. This improvement is critical for sustained drug release and optimizing therapeutic efficacy, particularly in challenging environments like the acidic pH of TNBC tumors [36].

3.3.2. In vitro release profile.

The in vitro release profiles of BCP-NIO and BCP-PLGA-NIO were evaluated under physiological (pH 7.4) and acidic (pH 5.5) conditions to mimic systemic circulation and the tumor microenvironment, respectively. As shown in Figure 5, the release rate of BCP was significantly influenced by both the pH environment and the presence of PLGA modification.

Under physiological conditions (pH 7.4), BCP-NIO exhibited a cumulative release of 50.68 ± 2.61 % after 24 hours. A comparable release profile was observed under acidic conditions (pH 5.5), where BCP-NIO released 56.35 ± 7.03 %. This relatively high and non-selective release across both pH environments suggests a lack of specificity in the release mechanism of BCP-NIO. Such behavior may be attributed to the inherent instability of niosomes under prolonged incubation, leading to leakage of the encapsulated drug irrespective of environmental pH.

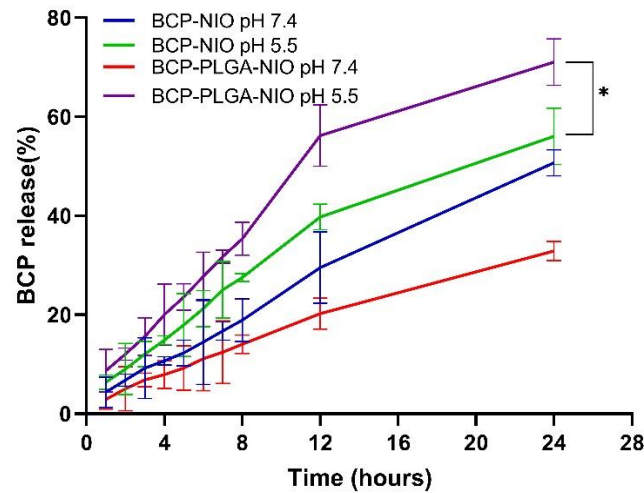


Figure 5. In vitro release profiles of BCP from niosomal formulations at pH 7.4 and pH 5.5. Data are presented as mean \pm SD (n = 3). Statistical significance was determined using an unpaired t-test: * p < 0.05 for BCP-PLGA-NIO compared to BCP-NIO at pH 5.5; non-significant (ns) for p \geq 0.05.

This non-specific release represents a major limitation for targeted drug delivery systems, as it increases the likelihood of premature drug release during systemic circulation, potentially reducing therapeutic efficacy and increasing off-target effects. In contrast, BCP-PLGA-NIO demonstrated a more controlled release profile, with a cumulative release of $32.89 \pm 1.91\%$ at pH 7.4, significantly lower than that of BCP-NIO under the same conditions. This behavior highlights the stabilizing effect of PLGA, which strengthens the niosomal structure and minimizes premature drug leakage in neutral environments. At pH 5.5, BCP-PLGA-NIO achieved a significantly enhanced release of $71 \pm 4.68\%$, which is higher than its release at pH 7.4 and markedly greater than the release observed for BCP-NIO under acidic conditions. This pH-sensitive release behavior can be attributed to the protonation of functional groups within the PLGA polymer in acidic environments, destabilizing the niosomal structure and facilitating the release of the encapsulated drug. Statistical analysis using an unpaired t-test revealed a significant difference between BCP-PLGA-NIO and BCP-NIO at pH 5.5 (p = 0.039), underscoring the superior performance of the PLGA-modified niosomal formulation in achieving targeted drug release in acidic, tumor-like conditions. The findings of this study align with previously reported behaviors of PLGA-based drug delivery systems, which facilitate controlled drug release in acidic environments mimicking the tumor microenvironment. For instance, Tripathi *et al.* demonstrated that PLGA-capped mesoporous silica nanoparticles significantly enhanced the release of capecitabine (CAP) at pH 6.8 compared to physiological pH. This enhanced release was attributed to the partial hydrolysis of the PLGA matrix under acidic conditions, destabilizing the nanoparticle structure and enabling efficient drug release [37]. Similarly, Li *et al.* reported that PLGA-TPGS nanoparticles exhibited a cumulative release of doxorubicin (DOX) of $58.59 \pm 4.71\%$ at pH 7.4, which increased to $66.59 \pm 1.48\%$ at pH 5.0 over 24 hours. [38]. This pH-dependent release was driven by the hydrolytic degradation of the PLGA segment in acidic environments. The behavior observed in BCP-PLGA-NIO is consistent with these studies, further validating the utility of PLGA as a material for pH-sensitive drug delivery. The non-specific release observed in BCP-NIO across both pH conditions highlights a critical limitation of conventional niosomes. Without pH-responsive functionality, BCP-NIO exhibited substantial leakage under physiological conditions, undermining its potential as a targeted delivery system. In contrast, BCP-PLGA-NIO displayed

dual functionality, with stability at physiological pH and enhanced release at acidic pH. This behavior directly addresses the limitations of conventional niosomes, enabling BCP-PLGA-NIO to function as a more precise and effective drug delivery system for hydrophobic compounds like BCP.

3.4. *In vitro* anti-TNBC evaluation.

The potential activity of BCP for combating TNBC previously predicted by an *in silico* study was validated by an *in vitro* experimental study. The cytotoxic effects of BCP and its encapsulated formulations were evaluated in 4T1 triple-negative breast cancer cells using the CCK-8 assay. The results, presented in Figure 6, demonstrate a significant improvement in anticancer efficacy with nanoencapsulation and further enhancement upon PLGA modification.

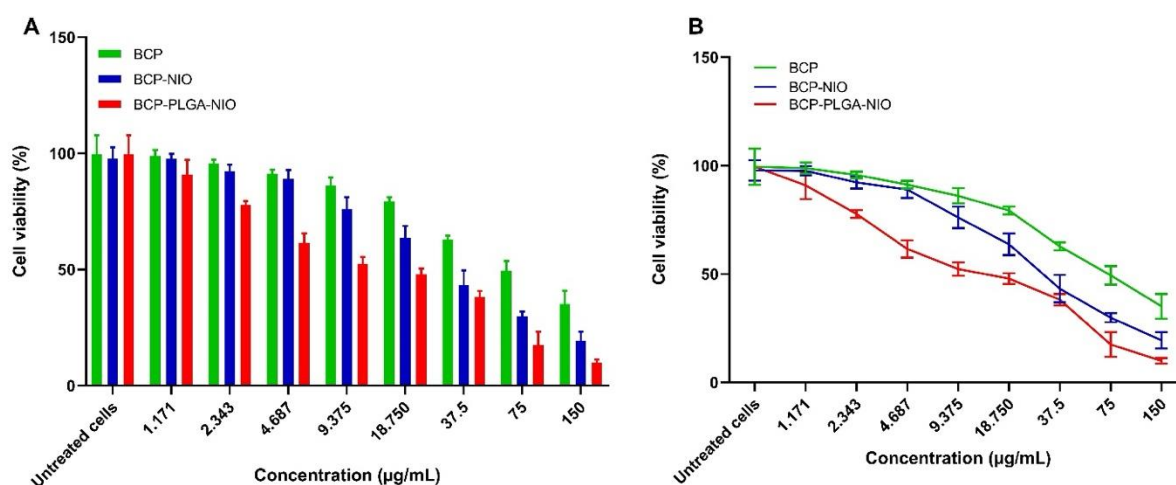


Figure 6. Cytotoxicity Assessment of Free BCP, BCP-NIO, and BCP-PLGA-NIO in 4T1 Breast Cancer Cells. (A) Histogram representation of cell viability (%) at varying concentrations (1.171–150 µg/mL) after 24 hours, evaluated using the CCK-8 assay; (B) Dose-response curves showing the concentration-dependent reduction in cell viability. Data are presented as mean ± SD (n = 3).

Free BCP exhibited moderate cytotoxicity, with an IC_{50} value of 72.068 ± 2.86 µg/mL. Encapsulation in niosomes significantly enhanced the anticancer activity, reducing the IC_{50} to 30.728 ± 1.48 µg/mL, corresponding to a 2.34-fold increase in efficacy compared to free BCP. This improvement highlights the role of niosomes in enhancing BCP's solubility, stability, and cellular uptake, overcoming the inherent limitations of the free compound [39]. BCP-PLGA-NIO demonstrated the most pronounced cytotoxic effects, achieving an IC_{50} of 15.647 ± 6.19 µg/mL, representing a 4.61-fold improvement compared to free BCP and a 1.96-fold enhancement over BCP-NIO. This substantial improvement can be attributed to the multifunctional properties of PLGA, which enhance encapsulation efficiency and enable pH-sensitive and on-demand drug release, thereby amplifying therapeutic effects. Across all tested concentrations, dose-dependent cytotoxicity curves (Figure 7A and 7B) show that BCP-PLGA-NIO elicited the steepest decline in cell viability, further underscoring its robust anticancer activity. The enhanced cytotoxicity observed with BCP-PLGA-NIO is directly related to its ability to overcome critical barriers in drug delivery.

PLGA undergoes protonation in acidic environments, such as those present in the tumor microenvironment and endosomal compartments, resulting in a charge reversal from negative to positive. This charge reversal destabilizes the endosomal membrane, enabling the

encapsulated drug to escape into the cytoplasm. Such efficient endosomal escape is essential for ensuring the therapeutic payload reaches its intracellular targets without being degraded or recycled within the endosomal-lysosomal pathway. These findings are consistent with previous research, such as the work of Panyam *et al.*, which demonstrated that PLGA-based nanoparticles effectively disrupt endosomal membranes in acidic conditions to enhance cytoplasmic delivery [40]. In addition to facilitating endosomal escape, PLGA contributes to controlled and pH-sensitive drug release. While remaining stable at physiological pH, PLGA undergoes hydrolysis and protonation in acidic environments, destabilizing the niosomal structure and triggering the release of the encapsulated drug. This dual behavior ensures that BCP is preferentially released in the acidic tumor microenvironment, allowing it to exert its cytotoxic effects more efficiently while minimizing systemic toxicity. The observed enhancement in cytotoxicity and selective drug release of BCP-PLGA-NIO highlights the potential of PLGA in developing advanced drug delivery systems. The significant reduction in IC₅₀ values compared to free BCP and BCP-NIO underscores the efficacy of PLGA modification in optimizing drug delivery through improved encapsulation, efficient endosomal escape, and controlled release. These findings suggest that PLGA-modified niosomes, such as TNBC, are well-suited to address the challenges of treating aggressive cancers. By precisely targeting the tumor microenvironment and ensuring efficient intracellular delivery, BCP-PLGA-NIO presents a promising platform for further preclinical investigations and potential clinical applications in cancer therapy.

However, developing such advanced delivery systems is critical in light of the limitations associated with conventional approaches. For instance, while liposomal formulations have been widely explored for delivering hydrophobic compounds like BCP, they face inherent limitations due to drug-membrane interactions that compromise delivery efficiency and therapeutic efficacy. Previous studies highlight that BCP interacts strongly with liposomal bilayers, particularly in unilamellar vesicles (ULVs), leading to drug entrapment within the lipid bilayer [41,42]. This interaction reduces drug bioavailability and release efficiency, ultimately limiting cytotoxic potential. Although multilamellar vesicles (MLVs) have been shown to improve drug loading by providing additional bilayer structures, their larger particle sizes hinder effective tumor penetration and circulation stability. These limitations necessitate the development of alternative delivery systems. PLGA-modified niosomes offer a strategic advantage by combining the structural stability of niosomes with the pH-sensitive and controlled release capabilities imparted by PLGA. Unlike liposomes, PLGA-modified niosomes can be engineered to achieve nanoscale dimensions while maintaining optimal drug entrapment efficiency.

Additionally, the charge-reversal property of PLGA in acidic environments facilitates endosomal escape, a feature that is critical for delivering hydrophobic drugs like BCP to their intracellular targets. This behavior contrasts with the limitations of traditional liposomal systems, which often struggle to achieve effective cytoplasmic delivery of drugs such as BCP. In this study, we introduced a compelling *in silico* pathway analysis that highlights the anticancer activity of BCP through the inhibition of HSP90AA1 expression, providing insights into its molecular mechanisms. Additionally, we addressed the significant *in vitro* challenges associated with encapsulating BCP in nanocarriers. By leveraging niosomes and enhancing their performance through PLGA modification, we successfully developed a system capable of on-demand drug release, improved stability, and enhanced anticancer activity. The PLGA-modified niosomes overcame conventional delivery systems' limitations and demonstrated

efficient encapsulation, targeted release, and intracellular delivery of BCP. These findings establish a robust foundation for advancing PLGA-modified niosomes as a next-generation drug delivery platform, highlighting their potential to overcome key challenges in cancer therapy, such as targeted delivery and enhanced intracellular uptake. Given their promising in vitro performance, these results strongly advocate for further in vivo investigations, including studies using xenograft models, to rigorously validate their efficacy, safety, and therapeutic potential, thereby accelerating their translation into preclinical and clinical applications for aggressive cancers [43].

4. Conclusions

This study presents a significant advancement in targeted cancer therapy by developing and evaluating a pH-sensitive hybrid niosomal formulation of BCP for treating TNBC. Combining in silico predictions with in vitro validation, this work addresses critical drug delivery challenges while introducing a novel anticancer pathway for BCP. The in silico analyses identified HSP90AA1 as a key target for BCP, supported by molecular docking and dynamics simulations that demonstrated stable interactions and strong binding affinity. These findings highlighted a novel pathway for BCP's anticancer activity, offering a mechanistic insight into its role in modulating TNBC progression. Incorporating PLGA into niosomes significantly improved encapsulation efficiency, pH-sensitive release, and cytotoxicity against TNBC cells. The hybrid formulation achieved superior performance, with a 4.61-fold improvement in IC₅₀ compared to free BCP and a 1.96-fold enhancement over standard niosomes, demonstrating the efficacy of this delivery system in overcoming critical barriers such as endosomal escape and tumor targeting. This study bridges fundamental research with translational potential by integrating computational and experimental methodologies, establishing PLGA-modified niosomes as a robust platform for targeted drug delivery. These findings lay the groundwork for future preclinical and clinical investigations, positioning this formulation as a promising strategy for effectively treating TNBC and other aggressive malignancies.

Author Contributions

Conceptualization: E.S., A.S.; Methodology: E.S.; Investigation: E.S., N.H.; Formal analysis: E.S.; Resources: B.H.N., S.E.M.; Data curation: M.I.A.; Writing original draft: E.S.; Writing review and editing: E.S., A.S., M.I.A., F.D.A.; Visualization: F.D.A.; Supervision: A.S., E.S.; Project administration: A.S.; Funding acquisition: M.I.A., B.H.N., A.S. All authors have read and agreed to the published version of the manuscript.

Institutional Review Board Statement

Not applicable.

Informed Consent Statement

Not applicable.

Data Availability Statement

Data supporting the findings of this study are available upon reasonable request from the corresponding author.

Funding

This research was partially funded by LPPM Universitas Islam Negeri Alauddin with contract number 422, year 2024, under registration number 24101000009049.

Acknowledgments

The authors gratefully acknowledge the support of the Nanopharmacy Research Centre Laboratory, Department of Pharmacy, Universitas Islam Indonesia, and Lipoid GmbH (Ludwigshafen, Germany).

Conflicts of Interest

The authors declare no conflict of interest.

References

1. Dahham, S.S.; Tabana, Y.; Asif, M.; Ahmed, M.; Babu, D.; Hassan, L.E.; Ahamed, M.B.K.; Sandai, D.; Barakat, K.; Siraki, A.; Majid A.M.S.A. β -Caryophyllene Induces Apoptosis and Inhibits Angiogenesis in Colorectal Cancer Models. *Int. J. Mol. Sci.* **2021**, *22*, 10550, <https://doi.org/10.3390/ijms221910550>.
2. Mannino, F.; Pallio, G.; Corsaro, R.; Minutoli, L.; Altavilla, D.; Vermiglio, G.; Allegra, A.; Eid, A.H.; Bitto, A.; Squadrito, F.; Irrera N. Beta-Caryophyllene Exhibits Anti-Proliferative Effects through Apoptosis Induction and Cell Cycle Modulation in Multiple Myeloma Cells. *Cancers* **2021**, *13*, 5741, <https://doi.org/10.3390/cancers13225741>.
3. Kim, C.; Cho, S.K.; Kim, K.D.; Nam, D.; Chung, W.S.; Jang, H.J.; Lee, S.G.; Shim, B.S.; Sethi, G.; Ahn, K.S. β -Caryophyllene Oxide Potentiates TNF α -Induced Apoptosis and Inhibits Invasion through down-Modulation of NF-KB-Regulated Gene Products. *Apoptosis* **2014**, *19*, 708-711, <https://doi.org/10.1007/s10495-013-0957-9>.
4. Alberti, T.B.; Barbosa, W.L.R.; Vieira, J.L.F.; Raposo, N.R.B.; Dutra, R.C. (-)- β -Caryophyllene, a CB2 Receptor-Selective Phytocannabinoid, Suppresses Motor Paralysis and Neuroinflammation in a Murine Model of Multiple Sclerosis. *Int. J. Mol. Sci.* **2017**, *18*, 691, <https://doi.org/10.3390/ijms18040691>.
5. Khongthong, P.; Roseweir, A.K.; Edwards, J. The NF-KB Pathway and Endocrine Therapy Resistance in Breast Cancer. *Endocr Relat Cancer* **2019**, *26*, R369-R380, <https://doi.org/10.1530/ERC-19-0087>.
6. Dong, C.; Wu, J.; Chen, Y.; Nie, J.; Chen, C. Activation of PI3K/AKT/MTOR Pathway Causes Drug Resistance in Breast Cancer. *Front. Pharmacol.* **2021**, *12*, 628690, <https://doi.org/10.3389/fphar.2021.628690>.
7. Burris, H.A. Overcoming Acquired Resistance to Anticancer Therapy: Focus on the PI3K/AKT/MTOR Pathway. *Cancer Chemother. Pharmacol.* **2013**, *71*, 829-842, <https://doi.org/10.1007/s00280-012-2043-3>.
8. Mödinger, Y.; Knaub, K.; Dharsono, T.; Wacker, R.; Meyrat, R.; Land, M.H.; Petraglia, A.L.; Schön, C. Enhanced Oral Bioavailability of β -Caryophyllene in Healthy Subjects Using the VESIsorb® Formulation Technology, a Novel Self-Emulsifying Drug Delivery System (SEDDS). *Molecules* **2022**, *27*, 2860, <https://doi.org/10.3390/molecules27092860>.
9. Khan, R.; Irchhaiya, R. Niosomes: a potential tool for novel drug delivery. *J. Pharm. Investig.* **2016**, *46*, 195-204, <https://doi.org/10.1007/s40005-016-0249-9>.
10. Makadia, H.K.; Siegel, S.J. Poly Lactic-Co-Glycolic Acid (PLGA) as Biodegradable Controlled Drug Delivery Carrier. *Polymers* **2011**, *3*, 1377-1397, <https://doi.org/10.3390/polym3031377>.
11. Sadaqa, E.; Kurniawan, F.; Mudhakir, D. Sodium Oleate Functionalized Simvastatin Liposomes: Boosting Endosomal Escape and Anticancer Efficacy in Triple Negative Breast Cancer. *Res. Pharm. Sci.* **2025**, *20*, 188–206, <https://doi.org/10.4103/RPS.RPS>
12. Hopkins, A.L. Network pharmacology: the next paradigm in drug discovery. *Nat. Chem. Biol.* **2008**, *4*, 682-690, <https://doi.org/10.1038/nchembio.118>.
13. Zolghadri, S.; Asad, A.G.; Farzi, F.; Ghajarzadeh, F.; Habibi, Z.; Rahban, M.; Zolghadri, S.; Stanek, A. Span 60/Cholesterol Niosomal Formulation as a Suitable Vehicle for Gallic Acid Delivery with Potent In

- Vitro Antibacterial, Antimelanoma, and Anti-Tyrosinase Activity. *Pharmaceuticals* **2023**, *16*, 1680, <https://doi.org/10.3390/ph16121680>.
14. Peltonen, L.J.; Yliruusi, J. Surface Pressure, Hysteresis, Interfacial Tension, and CMC of Four Sorbitan Monoesters at Water-Air, Water-Hexane, and Hexane-Air Interfaces. *J. Colloid Interface Sci.* **2000**, *227*, 1-6, <https://doi.org/10.1006/jcis.2000.6810>.
 15. Safari Sharafshadeh, M.; Tafvizi, F.; Khodarahmi, P.; Ehtesham, S. Folic Acid-Functionalized PEGylated Niosomes Co-Encapsulated Cisplatin and Doxorubicin Exhibit Enhanced Anticancer Efficacy. *Cancer Nanotechnol.* **2024**, *15*, 14, <https://doi.org/10.1186/s12645-024-00252-8>.
 16. Sadaqa, E.; Utami, R.A.; Mudhakhir, D. In Vitro Cytotoxic and Genotoxic Effects of Phyllanthus Niruri Extract Loaded Chitosan Nanoparticles in TM4 Cells and Their Influence on Spermatogenesis. *Pharmacia* **2024**, *71*, 1–14, <https://doi.org/10.3897/pharmacia.71.e112138>.
 17. He, K.; Zheng, X.; Zhang, L.; Yu, J. Hsp90 Inhibitors Promote P53-Dependent Apoptosis through PUMA and Bax. *Mol. Cancer Ther.* **2013**, *12*, 2559–2568, <https://doi.org/10.1158/1535-7163.mct-13-0284>.
 18. Neckers, L.; Workman, P. Hsp90 Molecular Chaperone Inhibitors: Are We There Yet? *Clinical Cancer Research* **2012**, *18*, 64–76, <https://doi.org/10.1158/1078-0432.ccr-11-1000>.
 19. Condelli, V.; Crispo, F.; Pietrafesa, M.; Lettini, G.; Matassa, D.S.; Esposito, F.; Landriscina, M.; Maddalena, F. HSP90 Molecular Chaperones, Metabolic Rewiring, and Epigenetics: Impact on Tumor Progression and Perspective for Anticancer Therapy. *Cells* **2019**, *8*, 532, <https://doi.org/10.3390/cells8060532>.
 20. Tian, Y.; Wang, C.; Chen, S.; Liu, J.; Fu, Y.; Luo, Y. Extracellular Hsp90 α and Clusterin Synergistically Promote Breast Cancer Epithelial-to-Mesenchymal Transition and Metastasis via LRP1. *J. Cell Sci.* **2019**, *132*, <https://doi.org/10.1242/jcs.228213>.
 21. Eisa, N.H.; Crowley, V.M.; Elahi, A.; Kommalapati, V.K.; Serwetnyk, M.A.; Llbiyi, T.; Lu, S.; Kainth, K.; Jilani, Y.; Marasco, D.; El Andaloussi A.; Lee, S.; Tsai, F.T.F.; Rodriguez, P.C.; Munn, D.; Celis, E.; Korkaya, H.; Debbab, A.; Blagg, B.; Chadli, A. Enniatin A Inhibits the Chaperone Hsp90 and Unleashes the Immune System against Triple-Negative Breast Cancer. *iScience* **2023**, *26*, 108308, <https://doi.org/10.1016/j.isci.2023.108308>.
 22. Utami, N.; Susianti, S.; Bakri, S.; Kurniawan, B.; Setiawansyah, A. Cytotoxic Activity of Cyperus Rotundus L. Rhizome Collected from Three Ecological Zones in Lampung-Indonesia against HeLa Cervical Cancer Cell. *J. Appl. Pharm. Sci.* **2023**, *13*, 141–148, <https://doi.org/10.7324/JAPS.2023.113764>.
 23. Wright, L.; Barril, X.; Dymock, B.; Sheridan, L.; Surgenor, A.; Beswick, M.; Drysdale, M.; Collier, A.; Massey, A.; Davies, N.; Fink, A.; Fromont, C.; Aherne, W.; Boxall, K.; Sharp, S.; Workman, P.; Hubbard, R.E. Structure-Activity Relationships in Purine-Based Inhibitor Binding to HSP90 Isoforms. *Chem. Biol.* **2004**, *11*, 775–785, <https://doi.org/10.1016/j.chembiol.2004.03.033>.
 24. Dernovšek, J.; Zajec, Ž.; Poje, G.; Urbančič, D.; Sturtzel, C.; Goričan, T.; Grissenberger, S.; Ciura, K.; Wozniński, M.; Gedgudas, M.; Zubriene, A.; Grdadolnik, S.G.; Mlinarič-Raščan, I.; Rajic, Z.; Cotman, A.E.; Zidar, N.; Distel, M.; Tomašič, T. Exploration and Optimisation of Structure-Activity Relationships of New Triazole-Based C-Terminal Hsp90 Inhibitors towards in Vivo Anticancer Potency. *Biomed. Pharmacother.* **2024**, *177*, 11694, <https://doi.org/10.1016/j.biopha.2024.116941>.
 25. Susianti, S.; Bahri, S.; Hadi, S.; Setiawansyah, A.; Rachmadi, L.; Fadilah, I.; Ratna, M.G. Integrating The Network Pharmacology and Molecular Docking Confirmed with In Vitro Toxicity to Reveal Potential Mechanism of Non-Polar Fraction of Cyperus Rotundus Linn as Anti-Cancer Candidate. *J. Multidiscip. Appl. Nat. Sci.* **2024**, *5*, 56-73, <https://doi.org/10.47352/jmans.2774-3047.228>.
 26. Smith, R.D.; Engdahl, A.L.; Dunbar, J.B.; Carlson, H.A. Biophysical Limits of Protein-Ligand Binding. *J. Chem. Inf. Model.* **2012**, *52*, 2098–2106, <https://doi.org/10.1021/ci200612f>.
 27. Caro, J.A.; Harpole, K.W.; Kasinath, V.; Lim, J.; Granja, J.; Valentine, K.G.; Sharp, K.A.; Wand, A.J. Entropy in Molecular Recognition by Proteins. *Proc. Natl. Acad. Sci. U.S.A.* **2017**, *114*, 6563–6568, <https://doi.org/10.1073/pnas.1621154114>.
 28. Sargsyan, K.; Grauffel, C.; Lim, C. How Molecular Size Impacts RMSD Applications in Molecular Dynamics Simulations. *J. Chem. Theory Comput.* **2017**, *13*, 1518–1524, <https://doi.org/10.1021/acs.jctc.7b00028>.
 29. Lobanov, M.Yu.; Bogatyreva, N.S.; Galzitskaya, O. V Radius of Gyration as an Indicator of Protein Structure Compactness. *Mol. Biol.* **2008**, *42*, 623–628, <https://doi.org/10.1134/S0026893308040195>.
 30. Kaushik, S.; Chang, C.-E. Molecular Mechanics Study of Flow and Surface Influence in Ligand-Protein Association. *Front. Mol. Biosci.* **2021**, *8*, 659687, <https://doi.org/10.3389/fmolb.2021.659687>.
 31. Bartlett, P.; Yusuff, N.; Rico, A.; Lindvall, M. Antihydrophobic Solvent Effects: An Experimental Probe for the Hydrophobic Contribution to Enzyme-Inhibitor Binding. *J. Am. Chem. Soc.* **2002**, *124*, 3853–3857, <https://doi.org/10.1021/JA012483S>.
 32. Päslock, C.; Schäfer, L.; Heyden, M. Protein Flexibility Reduces Solvent-Mediated Friction Barriers of Ligand Binding to a Hydrophobic Surface Patch. *Phys. Chem. Chem. Phys.* **2021**, *23*, 5665-5672, <https://doi.org/10.1039/d1cp00181g>.

33. Sun, Y.-F.; Xia, Z.; Zhao, Q.; Zheng, B.; Zhang, M.; Ying, Y. Insights Into the Resistance Mechanisms of Inhibitors to FLT3 F691L Mutation via an Integrated Computational Approach. *Front. Pharmacol.* **2019**, *10*, 1050, <https://doi.org/10.3389/fphar.2019.01050>.
34. Rana, N.; Singh, A.K.; Shuaib, M.; Gupta, S.; Habiballah, M.; Alkhanani, M.; Haque, S.; Reshi, M.S.; Kumar, S. Drug Resistance Mechanism of M46I-Mutation-Induced Saquinavir Resistance in HIV-1 Protease Using Molecular Dynamics Simulation and Binding Energy Calculation. *Viruses* **2022**, *14*, 697, <https://doi.org/10.3390/v14040697>.
35. Hernández-Giottonini, K.Y.; Rodríguez-Córdova, R.J.; Gutiérrez-Valenzuela, C.A.; Peñuñuri-Miranda, O.; Zavala-Rivera, P.; Guerrero-Germán, P.; Lucero-Acuña, A. PLGA Nanoparticle Preparations by Emulsification and Nanoprecipitation Techniques: Effects of Formulation Parameters. *RSC Adv.* **2020**, *10*, 4218-4231, <https://doi.org/10.1039/C9RA10857B>.
36. Chatterjee, M.; Chanda, N. Formulation of PLGA Nanocarriers: Specialized Modification for Cancer Therapeutic Applications. *Mater Adv* **2022**, *3*, 837-858, <https://doi.org/10.1039/D1MA00600B>.
37. Tripathi, A.D.; Labh, Y.; Katiyar, S.; Singh, A.K.; Chaturvedi, V.K.; Mishra, A. Folate-Mediated Targeting and Controlled Release: PLGA-Encapsulated Mesoporous Silica Nanoparticles Delivering Capecitabine to Pancreatic Tumor. *ACS Appl. Bio. Mater.* **2024**, *7*, 7838-7851, <https://doi.org/10.1021/acsabm.4c00019>.
38. Li, Z.; Qiu, L.; Chen, Q.; Hao, T.; Qiao, M.; Zhao, H.; Zhang, J.; Hu, H.; Zhao, X.; Chen, D.; Mei, L. PH-Sensitive Nanoparticles of Poly(L-Histidine)-Poly(Lactide-Co-Glycolide)-Tocopheryl Polyethylene Glycol Succinate for Anti-Tumor Drug Delivery. *Acta Biomater.* **2015**, *11*, <https://doi.org/10.1016/j.actbio.2014.09.014>.
39. Liga, S.; Paul, C.; Moacă, E.A.; Péter, F. Niosomes: Composition, Formulation Techniques, and Recent Progress as Delivery Systems in Cancer Therapy. *Pharmaceutics* **2024**, *16*, 223, <https://doi.org/10.3390/pharmaceutics16020223>.
40. Panyam, J.; Zhou, W.; Prabha, S.; Sahoo, S.K.; Labhasetwar, V. Rapid Endo-lysosomal Escape of Poly(DL-lactide- Co Glycolide) Nanoparticles: Implications for Drug and Gene Delivery. *FASEB J.* **2002**, *16*, 1217-1226, <https://doi.org/10.1096/fj.02-0088com>.
41. Di Sotto, A.; Paolicelli, P.; Nardoni, M.; Abete, L.; Garzoli, S.; Di Giacomo, S.; Mazzanti, G.; Casadei, M.A.; Petralito, S. SPC Liposomes as Possible Delivery Systems for Improving Bioavailability of the Natural Sesquiterpene β -Caryophyllene: Lamellarity and Drug-Loading as Key Features for a Rational Drug Delivery Design. *Pharmaceutics* **2018**, *10*, 274, <https://doi.org/10.3390/pharmaceutics10040274>.
42. Yakimov, I.D.; Kolmogorov, I.M.; Le-Deygen, I.M. Beta-Caryophyllene Induces Significant Changes in the Lipid Bilayer at Room and Physiological Temperatures: ATR-FTIR Spectroscopy Studies. *Biophysica* **2023**, *3*, 501-512, <https://doi.org/10.3390/biophysica3030033>.
43. Sadaqa, E.; Muhammad Ikhlas Arsul Xenograft Models for Preclinical Assessment of Anticancer Therapies: A Comprehensive Review. *Ad-Dawaa' J. Pharm. Sci.* **2023**, *6*, 1-16, <https://doi.org/10.24252/djps.v6i1.38677>.

Publisher's Note & Disclaimer

The statements, opinions, and data presented in this publication are solely those of the individual author(s) and contributor(s) and do not necessarily reflect the views of the publisher and/or the editor(s). The publisher and/or the editor(s) disclaim any responsibility for the accuracy, completeness, or reliability of the content. Neither the publisher nor the editor(s) assume any legal liability for any errors, omissions, or consequences arising from the use of the information presented in this publication. Furthermore, the publisher and/or the editor(s) disclaim any liability for any injury, damage, or loss to persons or property that may result from the use of any ideas, methods, instructions, or products mentioned in the content. Readers are encouraged to independently verify any information before relying on it, and the publisher assumes no responsibility for any consequences arising from the use of materials contained in this publication.